We have addressed all of the points raised by the reviewer (copied here and shown in black text), and include our responses to each point below (in blue text). Where there has been a major change in the manuscript we provide the original text (in black italics) and the new text (in blue italics).

1 Anonymous Referee 1

The manuscript deals with a methodology that can be used to derive the telescopic functions of a pulsed Doppler lidar. The idea is to use the information on the lidars telescopic functions to derive the attenuated backscatter profile from the SNR signal from the wind- lidar. The telescopic functions are estimated by comparing (by iteration) with the attenuated backscatter profile measured by a ceilometer.

After having read the paper several times I am still in doubt whether the methodology is intended for applied use or if is a purely academic exercise. I would like the authors to put more emphasis on the use of wind-lidars in practical applications for the measurements of attenuated backscatter profiles and what can achieved by such measurements from wind-lidars.

We have also included a statement outlining the advantage of obtaining attenuated backscatter and Doppler velocity measurements in the same measurement volume, with reference to the potential of deriving mass-fluxes, e.g. aerosol or cloud.

There is also an advantage to obtaining attenuated backscatter and Doppler velocity measurements in the same measurement volume, since this will simplify the calculation of cloud or aerosol mass-fluxes (Engelmann et al.*, 2008).*

1) It needs to be clarified why the data filtering is so strong, why are there so few good profiles out of so many available profiles in table 3. Are some of these data simply considered outliers - it is always dangerous to neglect outliers.

The majority of the filtering is to remove profiles that are not suitable for this method - profiles that contain clouds, precipitation or multiple aerosol layers (some sites are more cloudy than others). This explains the reduction of 'available profiles' to 'total estimates'. Then, the outlier filtering using MAD is the difference between 'total' and 'good estimates' and is usually $< 10\%$, except for the NSA site. The SNR for both instruments is quite low at NSA due to the low aerosol loading; hence the outlier filtering is stronger. The outliers are still plotted in Fig. 3 but not used in calculating the uncertainties.

2) How much does the improved telescopic functions improve the attenuated backscatter profile as compared to the information from the factory setting of the telescopic functions?

This will vary from instrument to instrument. D is often quite close to the nominal value provided by the manufacturer, but f may not be or may be unknown, and for some models, f can also be adjusted by some known or unknown amount by the operator.

3) How well does the attenuated backscatter profiles determined from the wind lidar SNR profile compare to the profiles observed by ceilometer. Only a few examples are shown in the paper, and a real quantification based on many (all) profiles from these rich data sets would be an considerable improvement to the paper. The main question is if the wind lidar is able on a routine basis to produce reliable profiles of attenuated backscatter profiles. A ceilometer is a very cheap instrument compared to a wind lidar, is it still recommendable to have a ceilometer next to a wind lidar or can the ceilometer be omitted and the backscatter profile determined with sufficient accuracy from the SNR?

The absolute values of the attenuated backscatter from the Doppler lidar and the ceilometer are not expected to be the same due to the difference in the wavelength, but for a homogeneous aerosol layer, the profile shape will match. The Doppler lidar is expected to then provide reliable profiles on a routine basis after applying the telescope focus function calculated using this method together with a calibration factor calculated using e.g. (Westbrook et al., 2010a).

Calculation of the telescope focus function can be made from a short time-series next to a ceilometer; the instrument can then be moved to another location, for campaigns for example. In practice this method can be performed during commissioning, and in principle, the manufacturer could also provide this service.

1.1 Minor remarks

1. Line 28 – page 5. Why is the threshold chosen to be 22.2 dB, the number sounds arbitrary. Why not simply set a very high threshold value for this exercise – e. g. -15 dB, to secure high quality data?

   The threshold is based on the SNR limit in Manninen et al.(2016) as the data we used has been processed with the same method. This threshold is based on the expected noise floor for the instruments considered here (Halo Streamline and Streamline XR) and should probably be modified for different instruments. A citation for the threshold has been added. We agree that a higher threshold could be used to secure high quality data, but we also wanted to test the applicability of the method in situations where mostly low SNR is expected, e.g. at the NSA site in Alaska where the aerosol loading is very low.

2. Line 28 page 5, If observations below -22.2 dB are discarded, the averaged SNR will be biased – is this accounted for?

   The order of these two steps was written incorrectly in the manuscript. The averaging was done prior to discarding the low SNR data, and the threshold then applied to the averaged data. The manuscript has now been corrected.

Before input, the Doppler lidar SNR data had a background correction applied to reduce bias (Manninen et al., 2016), and data below a minimum SNR threshold of -22.2 dB was discarded. Then, both ceilometer and Doppler lidar data were averaged to a common 30-minute, 30 m vertical resolution grid, using interpolation where necessary (only for one period from Darwin).

Before input, the Doppler lidar SNR data had a background correction applied to reduce bias (Manninen et al., 2016). Both ceilometer and Doppler lidar data were averaged to a common 30-minute, 30 m vertical resolution grid, using linear interpolation where necessary (only for one period from Darwin). After averaging, data below a minimum threshold of -22.2 dB (Manninen et al., 2016) was discarded.

3. Line 29 page 5. Explain what is meant by "using interpolation where necessary".

   Interpolation may necessary to get the ceilometer and Doppler lidar data on the same vertical grid. Usually, the vertical resolution of the ceilometer data is high enough (10 m) so that 2 or 3 range gates in the vertical can be summed to match the Doppler lidar vertical resolution, however at one site the difference between the vertical resolutions of the two instruments required linear interpolation between ceilometer range gates to match the Doppler lidar resolution.

4. Line 9 page 6. How is the cloud base detected? Do you use a threshold method (if yes what is the threshold) or a more sophisticated method?

   Here we use the Vaisala cloud base detection, which uses a gradient method on the ceilometer attenuated backscatter profile. A more sophisticated shape method (e.g. Tuononen et al., 2019) could also be used but we are not so interested in the precise cloud base value, more whether a cloud layer exists in the profile - this is also why we only use data more than 150 m below cloud base.

5. Line 17, Page 8: Explain why you expect f-2 to be superior.

   When examining Equation (2), we expect f-2 to be superior to f, and f-2 is closer to the distribution observed for the telescope focus in figure 3. Additionally, figure 1a, which is plotted with range in logarithmic units also suggests this relationship.

6. Why do you mix two parameters for the flagging in Eq. (8), It seems more natural to flag the individual parameter.

   Our best estimate for the Telescope Focus Function parameters is the peak of the bi-variate (f,D) distribution, and thus for the flagging we use distance from the peak of the bi-variate distribution.

2 Anonymous Referee 2

2.1 General comments

The paper presents a practical method for characterizing the "telescope aperture function" of a pulse heterodyne lidar. As explained in the article, this function is required to correct the intensity of the signals recorded by the instrument (termed SNR as it is normalized to the level of white noise in the heterodyne lidar) from the variations of the instrument sensitivity with the range. This function is more complicated than with a direct-detection aerosol lidar as it is not given by the overlap between the laser beam and the telescope aperture, but has more to do with the efficiency of the heterodyne detection. However, an expression exists that predicts how it varies with the range as a function of two system parameters, namely the size of the telescope aperture D and the focal length f. The idea is to tune these two parameters until the corrected signal intensities match the attenuated backscatter measured by a nearby ceilometer. Of course, this method requires the presence of ceilometer nearby, but ceilometers are rather cheap instruments, and are deployed in great numbers in meteorological observation networks. The method opens the possibility to use a heterodyne wind lidar as an aerosol lidar and thus combine with a unique instrument the measurement of wind and aerosol backscatter profiles. This is of great interest for the characterization of pollution transport or the study of the atmospheric boundary layer.

There are several limitations to the method. One deals with the difference of the laser wavelength of a ceilometer (usually close to $0.9\mu m$) and a pulsed heterodyne lidar ($\lambda \approx 1.5\mu m$). The value of the attenuated backscatter are different at the two wavelengths, and the difference is dependant of the nature the aerosols. The method would thus be in trouble if several layers of different aerosols are present in the laser beam. This limitation is clearly discussed in the text. There is, however, a second limitation. The heterodyne efficiency does not depend solely of the instrument parameters, but also on the optical turbulence. This dependency appears in equation (2) of the article with the ρ_0 parameter. It is assumed in article that ρ_0 >> D so that its effect on $A_e(R)$ can be neglected. This assumption is not justified. In practice, it can happen that the turbulence significantly degrades the heterodyne efficiency of the lidar. This is particularly the case when the beam is directed horizontally, a few meters above the ground, on a hot, sunny day. In the article, the vertical (or close to vertical) direction of the beam should alleviate the degradation as the optical turbulence drops very rapidly with the altitude, but it would be worth to have a short calculation of ρ_0 as a function of the range using a typical profile of ${C_n}^2$ and the formulation of Frehlich and Kavaya for ρ_0 (equation 165).

This is a very good point. Discussion of the impact of refractive turbulence has been added as a new subsection 4.3 together with an additional figure (figure 7 in the new manuscript).

So far we have neglected the potential impact of turbulence on $T_f(R)$ arising

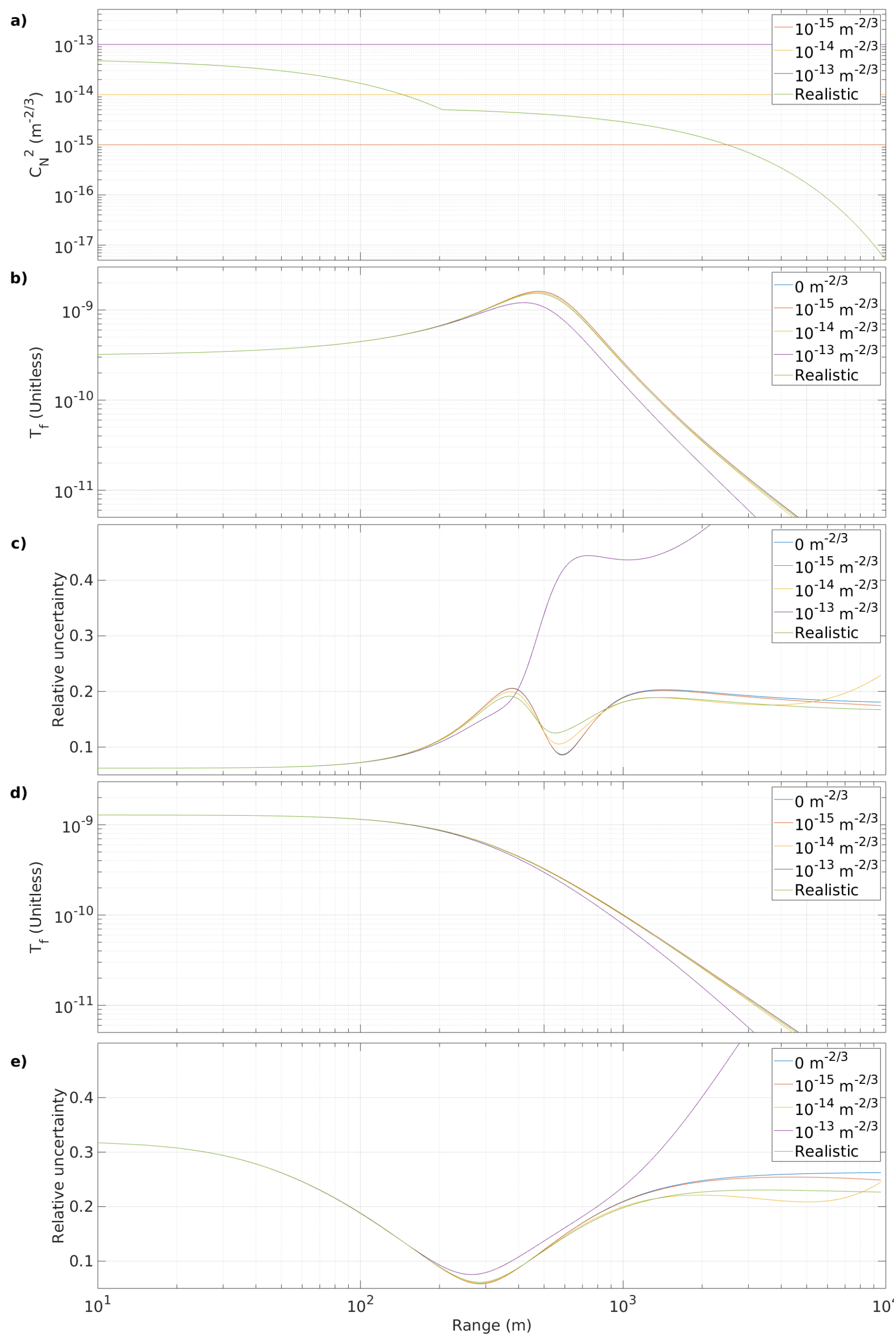

Figure 1: Impact of turbulent parameter, ρ_0, on telescope focus function, $T_f(R)$ and relative uncertainties, $\sigma_{T_f}(R)$, for different ${C_n}^2$ profiles. a) selected profiles of ${C_n}^2$ with range; b) $T_f(R)$ and c) $\sigma_{T_f}(R)$ for Darwin, 21 June 2011 to 22 July 2012; d) $T_f(R)$ and e) $\sigma_{T_f}(R)$ for NSA 30 July 2014 to 31 December 2017.

from the refractive turbulent parameter, ρ_0, in (2). An expression for ρ_0 is given in (Frehlich and Kavaya, 1991),

$$\rho_0(R) = [Hk^2 \int_0^R {C_n}^2(z)(1 - z/R)^{5/3} dz]^{-3/5}, \quad (1)$$

where $H = 2.914383$, $k = 2\pi/\lambda$, and ${C_n}^2(z)$ is the refractive turbulence at range z. We chose 3 profiles with constant ${C_n}^2(z)$, and a realistic vertical profile based on the most turbulent case presented by (Roadcap and Tracy, 2009). Figure 1 shows the impact that these different profiles have on $T_f(R)$, and the resulting re-sampling calculation of $\sigma_{T_f}(R)$ for two Doppler lidar instruments with different $T_f(R)$. Values of ${C_n}^2$ up to $10^{-14}m^{-2/3}$ have negligible impact on $T_f(R)$, and even the realistic profile only showed a slight increase in $\sigma_{T_f}(R)$ for the instrument with a focus set closer than infinity. This suggests that the impact of turbulence can be safely neglected for low values of ${C_n}^2$, and for most applications, can also be neglected when operating in the vertical. Hence, turbulence has no significant impact on the methodology described here for deriving the parameters f and D and their uncertainties from vertical profiles, but can be included for completeness.

However, it is clear that the turbulent impact should not be ignored when measuring at low elevation angles close to the horizon, where a profile similar to ${C_n}^2 = 10^{-13}m^{-2/3}$ may be possible. Fig. 1 shows that such a profile has a major impact on $T_f(R)$, especially in the far range. In these cases, the parameters f and D obtained from vertical measurements are still applicable, but $\rho_0(R)$ must also be calculated or estimated in order to derive the profile of attenuated backscatter, $\beta'(R)$.

An additional paragraph has been added to the conclusion.

The impact of turbulence on $T_f(R)$ was also investigated and was found to have no significant impact on the methodology described here for deriving the parameters f and D and their uncertainties from vertical profiles. However, the turbulent impact should not be ignored when measuring at low elevation angles close to the horizon, as it can modify $T_f(R)$ considerably, especially in the far range. In these cases, the parameters f and D obtained from vertical measurements are still applicable, but the turbulent contribution to $T_f(R)$ should included when deriving the attenuated backscatter coefficient.

It is written in the abstract that the method proposed in the article is applicable to Halo Photonics heterodyne Doppler lidars. It is clear that it is tested on data from Halo Photonics lidars, but I do not see why it could not be applicable to heterodyne lidars from other manufacturers as long as they provide measurements of SNR. If that is true, it would be worth mentioning it in the abstract as it widens the applicability of the method.

This is correct, and is now mentioned in the abstract and the conclusion.

Here, we present a methodology for deriving the telescope focus function *using a co-located ceilometer for pulsed heterodyne Doppler lidars. The method was tested with Halo Photonics Streamline and Streamline XR Doppler lidars, but should also be applicable to other pulsed heterodyne Doppler lidar systems.*

We have developed a method for deriving the telescope focus function and its uncertainty for pulsed heterodyne Doppler lidars, and applied the method to Halo Photonics Streamline and XR Doppler lidars.

2.2 Specific comments

1. In the paragraph that follows equation (1), the meaning of the η term is not explained.

   η is the detector quantum efficiency has been added to the text.

2. Equation (5): the equation applies to relative uncertainties. This shall be made clear.

   We have clarified this in the text.

3. Line 28: why this -22.2dB SNR threshold?

   The threshold is based on the SNR limit in Manninen et al.(2016) as the data we used has been processed with the same method. This threshold is based on the expected noise floor for the instruments considered here (Halo Streamline and Streamline XR) and should probably be modified for different instruments. A citation for the threshold has been added.

4. Table 4 on page 13: the meaning of b in N(f-2, b) and N(f, b) is not explained in the legend.

   The term b was a mistake, it is supposed to be D. This has now been corrected.

References

M. Tuononen, E. J. O'Connor, and V. A. Sinclair: Evaluating solar radiation forecast uncertainty, *Atmos. Chem. Phys.*, **19**, 1985–2000, doi:10.5194/acp-19-1985-2019, 2019.

Engelmann, R., Wandinger, U., Ansmann, A., Müller, D., Žeromskis, E., Althausen, D., and Wehner, B.: Lidar Observations of the Vertical Aerosol Flux in the Planetary Boundary Layer, Journal of Atmospheric and Oceanic Technology, 25, 1296–1306, doi:10.1175/2007JTECHA967.1, 2008.

Methodology for deriving the telescope focus function and its uncertainty for a heterodyne pulsed Doppler lidar

Pyry Pentikäinen[1], Ewan James O'Connor[2,3], Antti Juhani Manninen[2], and Pablo Ortiz-Amezcua[4,5]

[1]Institute for Atmospheric and Earth System Research / Physics, Faculty of Science, University of Helsinki, Helsinki, Finland
[2]Finnish Meteorological Institute, Helsinki, Finland
[3]Department of Meteorology, University of Reading, United Kingdom
[4]Andalusian Institute for Earth System Research (IISTA-CEAMA), 18006, Granada, Spain
[5]Department of Applied Physics, University of Granada, 18071 Granada, Spain

Correspondence: Pyry Pentikäinen (pyry.pentikainen@helsinki.fi)

Abstract. Doppler lidars provide two measured parameters, radial velocity and signal-to-noise ratio, from which winds and turbulent properties are routinely derived. Attenuated backscatter, which gives quantitative information on aerosols, clouds, and precipitation in the atmosphere, can be used in conjunction with the winds and turbulent properties to create a sophisticated classification of the state of the atmospheric boundary layer. Calculating attenuated backscatter from the signal-to-noise ratio requires accurate knowledge of the telescope focus function, which is usually unavailable. Inaccurate assumptions of the telescope focus function can significantly deform attenuated backscatter profiles, even if the instrument is focused at infinity. Here, we present a methodology for deriving the telescope focus function using a co-located ceilometer for pulsed heterodyne Doppler lidars. The method was tested with Halo Photonics Streamline and Streamline XR Doppler lidars, but should also be applicable to other pulsed heterodyne Doppler lidar systems. The method derives two parameters of the telescope focus function, the effective beam diameter and the effective focal length of the telescope. Additionally, the method provides uncertainty estimates for the retrieved attenuated backscatter profile arising from uncertainties in deriving the telescope function, together with standard measurement uncertainties from the signal-to-noise ratio. The method is best suited for locations where the absolute difference in aerosol extinction at the ceilometer and Doppler lidar wavelengths is small.

1 Introduction

Coherent Doppler lidar systems are capable of providing accurate radial Doppler velocities at high temporal and spatial resolution, and have been employed across a wide range of scientific and operational fields. Meteorological applications include the retrieval of turbulent properties to determine the strength, location and source of mixing in the atmospheric boundary layer, and, with many systems having scanning capability, the retrieval of winds. Information on the targets responsible for the radial Doppler velocities measured by the Doppler lidar (e.g. aerosol, cloud, precipitation), would greatly aid the interpretation of both the velocities and the products derived from them, but this requires quantitative use of the signal power received by the instrument.

The performance of a Doppler lidar depends on the signal-to-noise ratio, SNR, of the system, as SNR determines the radial velocity uncertainty (Rye and Hardesty, 1993; Pearson et al., 2009). The outgoing laser beam can be focused to improve the SNR at ranges close to the focal length (Pearson et al., 2002), and this is often used to improve the Doppler lidar velocity data quality and data availability, particularly in the atmospheric boundary layer. The optimal choice of focus will depend on the atmospheric conditions at the deployment location (Hirsikko et al., 2014).

Knowledge of how the choice of instrument parameters, such as the effective focal length of the telescope, impact the SNR profile is necessary in order to obtain profiles of attenuated backscatter coefficient (Zhao et al., 1990). A comprehensive overview of the theoretical considerations in determining the performance of coherent Doppler lidar systems was given by Frehlich and Kavaya (1991), who provided analytical expressions for deriving the expected signal measured by the coherent detector for a given target for a range of instrument configurations, including analytical expressions for the telescope focus function (also termed coherent responsivity). Most analytical expressions assume ideal Gaussian beams, which may not always be appropriate (Hill, 2018), hence experimental approaches have also been used to determine the impact of beam aberrations (Hu et al., 2013).

The profile of attenuated backscatter coefficient has the potential to be used in real time by weather forecasters (Illingworth et al., 2019), as it can be used in the same manner as for ceilometers. This includes the detection of liquid, supercooled-liquid, mixed-phase and ice clouds (Hogan et al., 2003; Van Tricht et al., 2014; Tonttila et al., 2015), aerosol layer and mixing-height determination (Flentje et al., 2010; Kotthaus and Grimmond, 2018), and retrieving precipitation parameters (Lolli et al., 2018).

In addition to providing velocity estimates for wind and turbulence, the inclusion of the profile of attenuated backscatter coefficient is advantageous for Doppler lidar boundary layer classification schemes (Tucker et al., 2009; Harvey et al., 2013; Manninen et al., 2018) by enhancing the discrimination between aerosol, cloud and precipitation, and can be used for tracking elevated aerosol plumes (Hannon et al., 1999). The combination of attenuated backscatter profiles from coherent Doppler lidars with other profiling instruments permits additional retrievals; for example, together with a ceilometer (Westbrook et al., 2010b), or with a cloud radar (Träumner et al., 2010), can yield drizzle drop size and precipitation rate. There is also an advantage to obtaining attenuated backscatter and Doppler velocity measurements in the same measurement volume, since this will simplify the calculation of cloud or aerosol mass-fluxes (Engelmann et al., 2008).

Therefore, an accurate profile of attenuated backscatter coefficient requires confidence in the parameters used to generate the telescope focus function. The parameters may not be known a priori, or may differ from what is assumed, and incorrect values can result in artefacts and very large biases in attenuated backscatter coefficient. We present a methodology for deriving the parameters of the telescope focus function experimentally from co-located Doppler lidar and ceilometer observations, together with the uncertainties in the function parameters. The ceilometer, for which the overlap function is known, provides our reference attenuated backscatter profiles. This methodology is relevant for coherent Doppler lidars designed for meteorological applications with maximum ranges suitable for observing the full extent of the boundary layer and beyond. Note that a calibration constant may still need to be determined and applied after implementing the calculated telescope focus function to retrieve the profile of attenuated backscatter coefficient (Westbrook et al., 2010a; Chouza et al., 2015).

The theoretical description of the telescope focus function is outlined in Sec. 2. In Sec. 3, we introduce the instruments and the methodology for deriving the parameters of the telescope focus function experimentally. An iterative least-squares regression using weighted-Mean-Square-Error (MSE) is used to find the best solution for the telescope focus function, where the weights represent the measurement uncertainties in both instruments. The use of long time periods (one year or more) also provides an estimate of the uncertainties in the parameters for the telescope focus function, which can then be propagated through to uncertainties in the retrieved attenuated backscatter coefficients. The methodology is applied to different instruments in multiple locations in Sec. 4 and the validation of the method is presented in Sec. 5.

2 Theory

2.1 Telescope focus function

Following Frehlich and Kavaya (1991), the coherent Doppler lidar equation can be expressed as

$$\mathrm{SNR}(R) = \frac{\eta c E}{2h\nu B}\frac{A_e(R)}{R^2}\beta'(R), \tag{1}$$

where SNR is the signal-to-noise ratio, varying as a function of range, R, from the instrument, β' is the attenuated backscatter coefficient, η is the detector quantum efficiency, c is the speed of light, E is the beam energy, h is Planck's constant, ν is the optical frequency, B is the receiver bandwidth, and A_e is the effective receiver area.

For a monostatic system emitting a circular Gaussian beam, using a circular aperture, and having matched filters, the effective receiver area is given by (Frehlich and Kavaya, 1991; Henderson et al., 2005)

$$A_e(R) = \frac{\pi D^2}{4\left(1+\left(\frac{\pi D^2}{4\lambda R}\right)^2\left(1-\frac{R}{f}\right)^2+\left(\frac{D}{2\rho_0}\right)^2\right)}, \tag{2}$$

where D is the $1/e^2$ effective diameter of a Gaussian beam, λ is the laser wavelength, f is the effective focal length of the telescope for the transmitter and receiver, and ρ_0 is a turbulent parameter, also termed transverse field coherence length.

Collecting the range-dependent terms, we obtain a unitless telescope focus function

$$T_f(R) = \frac{A_e(R)}{R^2}, \tag{3}$$

which is also termed the coherent responsivity (Frehlich and Kavaya, 1991).

The profile of attenuated backscatter coefficient is then obtained by rearranging (1)

$$\beta'(R) = \frac{2h\nu B}{\eta c E}\frac{\mathrm{SNR}(R)}{T_f(R)}. \tag{4}$$

Figure 1a shows how $T_f(R)$ depends on the telescope focal length, f, and Fig. 1b how $T_f(R)$ depends on D. Both figures show that the apparent focus — i.e range to the $T_f(R)$ maximum — is always closer than f, and that decreasing D shortens the apparent focus. This makes estimation of the parameters by eye in $T_f(R)$ prone to errors, since the apparent focus cannot be translated into f without knowledge of D.

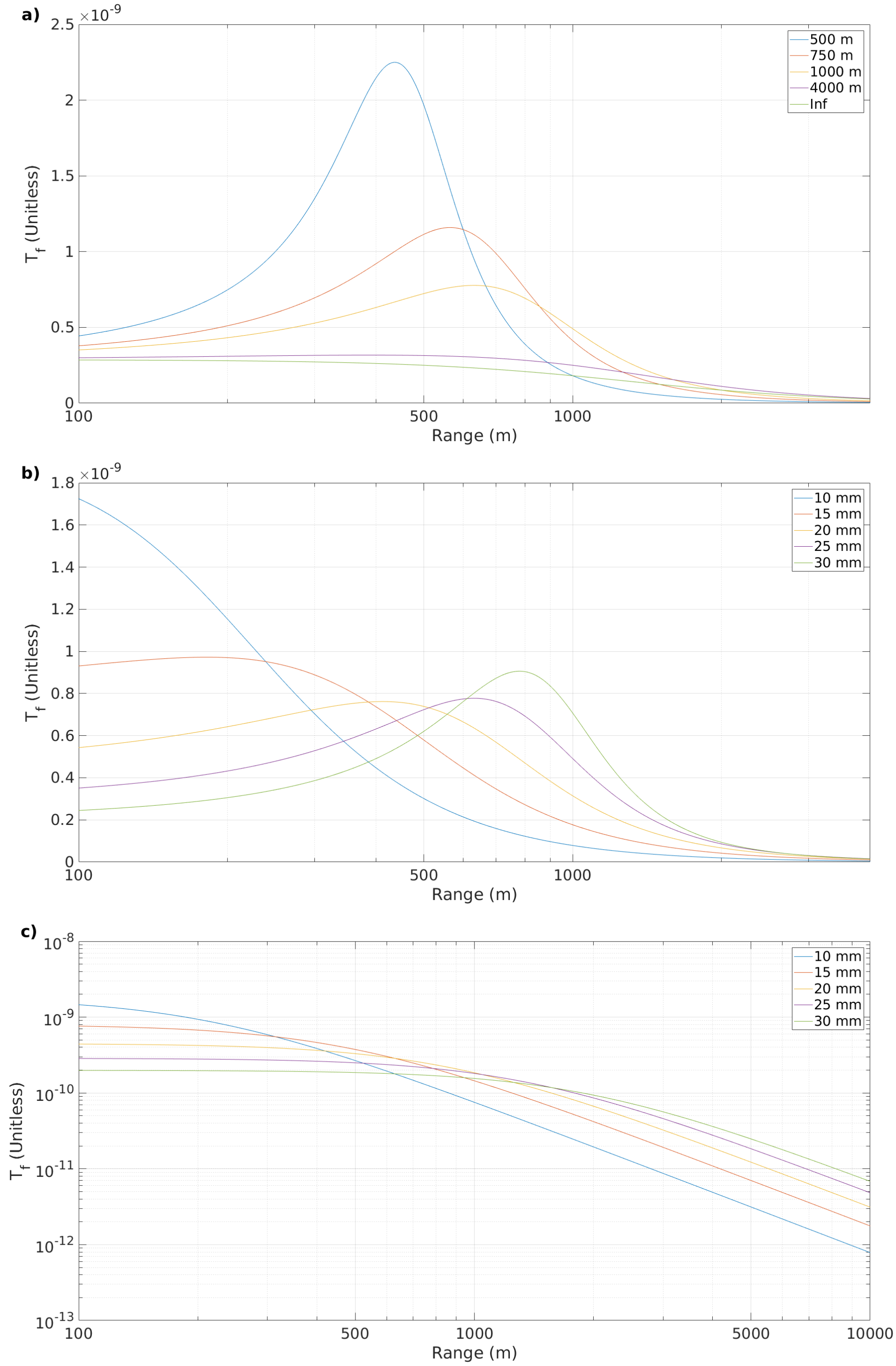

Figure 1. Telescope focus functions for: a) varying f with D=70 mm, b) varying D with f=1000 m, c) varying D with f being infinity.

Figure 1c shows that even if the telescope is focused at infinity, knowledge of the D is essential to derive attenuated backscatter coefficient profiles. While the gradient of $T_f(R)$ may be independent of D at the near and far ranges, the relative magnitude is not, and the potential variation is high in the range of the profile that is commonly of most interest.

2.2 Uncertainty in attenuated backscatter coefficient

Assuming that the parameters $T_f(R)$ and SNR are independent, and have uncertainties that can be described as Gaussian, the relative random uncertainty in attenuated backscatter coefficient is

$$\sigma_{\beta'} = \sqrt{{\sigma_S}^2 + {\sigma_{T_f}}^2}, \tag{5}$$

where σ_S is the relative uncertainty in the Doppler lidar SNR, and σ_{T_f} is the relative uncertainty in $T_f(R)$. An expression for deriving σ_S is given by Manninen et al. (2018), and we describe our method for obtaining σ_{T_f} in Section 4.2.

3 Application to data

There are 3 range-dependent unknowns in (2): f, D, and ρ_0. We assume that we can neglect ρ_0, and describe a method for estimating f and D, together with their uncertainties, which can then be propagated to obtain the uncertainty in the attenuated backscatter coefficient.

3.1 Instruments

We used measurements taken from the U.S. Department of Energy Atmospheric Radiation Measurement (ARM, Mather et al., 2016) observatories. We selected 5 sites with co-located ceilometer and Doppler lidar instruments: Southern Great Plains, US (SGP); Tropical West Pacific, Darwin, Australia (Darwin); Barrow, Alaska, US (NSA); Graciosa, Azores (Graciosa); Ascension Island, Atlantic, UK (Ascension).

The Doppler lidars operated by ARM comprise both Halo Photonics Streamline, and Streamline XR versions. These are commercially available heterodyne pulsed systems capable of full-hemispheric scanning and operated at a temporal resolution of 1-2 s (see Table 1). The focus for the Streamline version can be set by the operator, whereas the Streamline XR has the focus set by the manufacturer; however ARM has had some instruments upgraded from their original specification.

The ceilometer at all sites was a Vaisala CL31 ceilometer, which has a coaxial design and full overlap before 100 m and a temporal resolution of 30 s (more specifications given in Table 2).

3.2 Methodology

3.2.1 Telescope focus function parameter estimation

The methodology for deriving the parameters of the telescope focus function compares profiles from co-located Doppler lidar and ceilometer using an iterative least-squares regression to find the best solution. The method follows the process diagram given in Fig. 2.

Table 1. Halo Photonics Streamline and Streamline XR heterodyne Doppler lidar specifications. Values in parentheses refer to the specification of the Doppler lidar during the first period in Darwin.

Wavelength	1.5 μm
Pulse repetition rate	15 kHz
Nyquist velocity	19.8 m s^{-1}
Sampling frequency	50 MHz
Points per range gate	10 (16)
Range resolution	30 m (48 m)
Pulse duration	0.2 μs
Divergence	33 μrad
Antenna	monostatic optic-fibre coupled

Table 2. Vaisala CL31 ceilometer specifications.

Wavelength	910 nm
Pulse repetition rate	5.57 kHz
Range resolution	30 m
Lens diameter	14.5 cm
Divergence	0.75 mrad

Before input, the Doppler lidar SNR data had a background correction applied to reduce bias (Manninen et al., 2016). Both ceilometer and Doppler lidar data were averaged to a common 30-minute, 30 m vertical resolution grid, using linear interpolation where necessary (only for one period from Darwin). After averaging, data below a minimum threshold of -22.2 dB (Manninen et al., 2018) was discarded.

The data was then filtered to select only those portions of the profiles that are considered reliable for comparison. Ceilometer data below 195 m was discarded to ensure that only data with full overlap was used.

Due to the wavelength difference between the Doppler lidar and the ceilometer, it cannot be assumed that the atmospheric backscattering properties are the same at both wavelengths. However, we are only interested in the profile shape, not the absolute values, so profiles from the Doppler lidar and the ceilometer can be compared as long as they contain only one type of scatterer, and one which can be assumed to be distributed homogeneously throughout the portion of the profile used for comparison. Hence, the portion of a profile selected for comparison should contain only one aerosol layer, no clouds, and no precipitating hydrometeors.

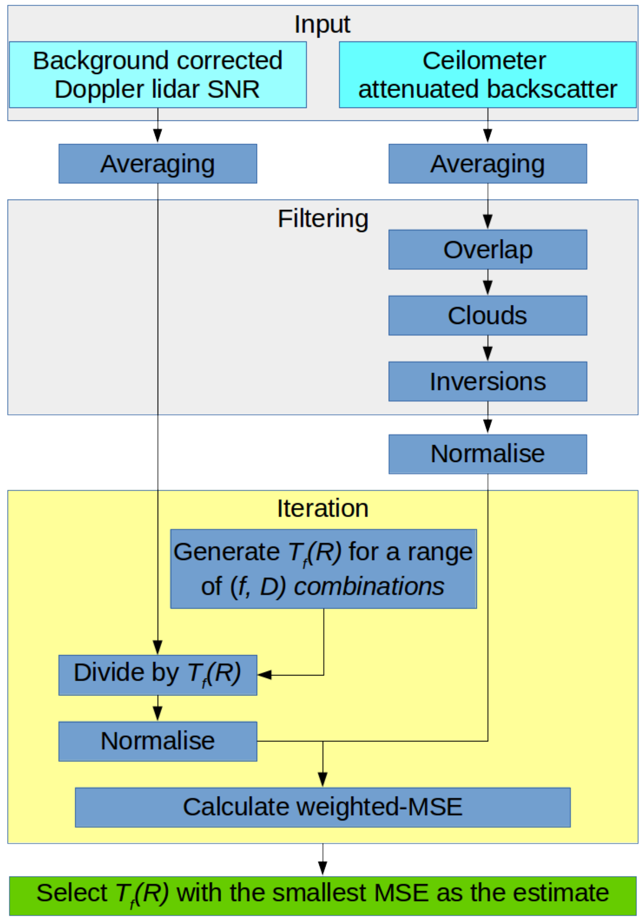

Figure 2. Process diagram of the telescope focus function parameter estimation.

We removed clouds by identifying the range gate 150 m below the cloud base detected by the ceilometer and excluding all data beyond this. Elevated aerosol layers and precipitating hydrometeors were filtered out by identifying layers using a convolution of the ceilometer profile with a haar-wavelet to detect changes in the gradient. The base of the second layer was identified where the gradient was increasing over 2 range gates and all data above this was discarded. This process also eliminates noisy profiles with low SNR.

The $T_f(R)$ parameter estimation is performed on a profile-by-profile basis for each profile where the filtering process leaves 8 successive range gates present. From equation 4, dividing the Doppler lidar SNR profile with the appropriate $T_f(R)$ will generate a Doppler lidar attenuated backscatter profile whose shape should match that of the ceilometer attenuated backscatter profile.

We use a brute-force approach to iterate through a range of reasonable f and D values, generating a corresponding $T_f(R)$ and Doppler lidar attenuated backscatter profile for each combination of values. The ceilometer profile and resulting Doppler lidar attenuated backscatter profiles are normalised so that the integral value of the unfiltered portion is unity. We then use a least-squares regression using weighted-MSE to find the best solution (smallest MSE), where the weights represent the measurement uncertainties in both instruments. Collecting results over many profiles results in a bi-variate distribution; the peak of this distribution is chosen as the best estimate of f and D, and hence the best estimate of $T_f(R)$ using (3).

3.2.2 Outlier removal

Occasionally, data of poor quality passes the filtering step in Fig. 2. The most common issues are noisy ceilometer data, and a bias in the Doppler lidar SNR profiles. If not screened, these occasional profiles result in significantly altered $T_f(R)$ estimation. Any noise in the ceilometer data is magnified by the profile length often being relatively short, and hence large uncertainty in even a single range gate can skew the regression. Doppler lidar SNR bias will impact the normalisation process, changing the $T_f(R)$ selected by the method due to the now incorrect profile shape. Due to the non-linearity of the $T_f(R)$ parameter estimation process, these issues result in regression solutions wildly inconsistent with the estimates based on good data. These outliers, which do not fall within the normal uncertainty observed in good data, are then removed from the bi-variate distribution of solutions before calculating the uncertainty estimates.

We used the median absolute deviation, MAD (Huber and Ronchetti, 2009; Leys et al., 2013), to distinguish outliers in the bivariate distribution of estimated f and D. MAD can be calculated using

$$MAD = b\, med\{|x_i - med\{x_i\}|\}, \tag{6}$$

where $b = 1.4826$ when the distribution excluding the outliers is normal. However, the distribution of f and D may not meet this criterion due to the non-linearity of $T_f(R)$ and the computational $T_f(R)$ estimation process. We expect the distributions of D and f^{-2} to be close to normal and will use f^{-2} rather than f to determine outliers. Additionally, the peak of the bi-variate distribution may not always coincide with the medians of the uni-variate D and f^{-2} distributions, and, hence, we use a modified form of (6),

$$MAD = b\, med\{|x_i - peak\{x_i, y_i\}|\}. \tag{7}$$

We selected 3 MADs as the threshold for flagging outliers:

$$\sqrt{\left(\frac{f_i^{-2} - med\{f_i^{-2}\}}{MAD_{f^{-2}}}\right)^2 + \left(\frac{D_i - med\{D_i\}}{MAD_D}\right)^2} \geq 3. \tag{8}$$

Assuming the distribution excluding the outliers to be normal, 3 MADs correspond to 3 standard deviations of the underlying distribution. In cases where f is at infinity, all estimates with a finite f will be flagged as outliers.

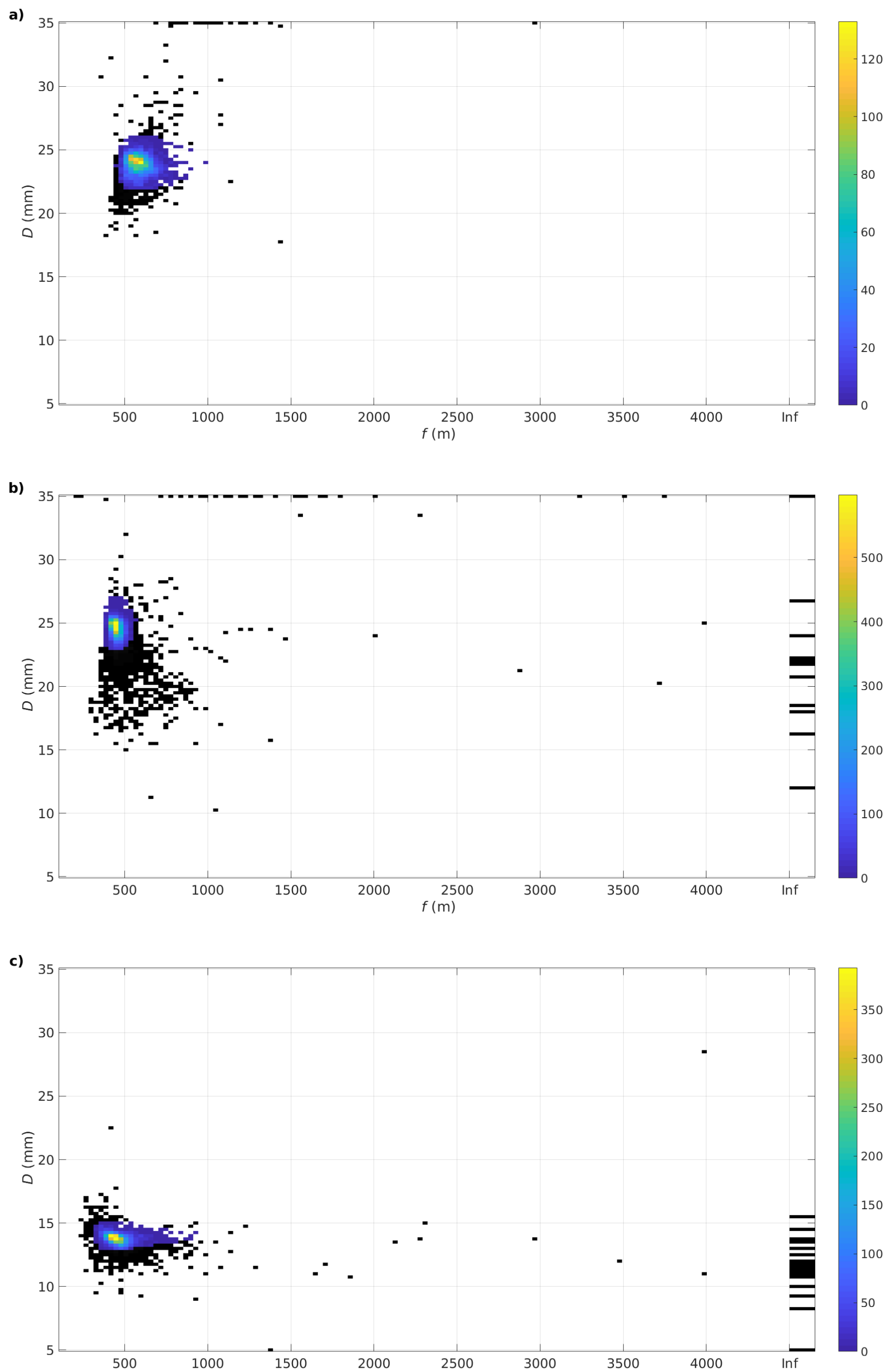

Figure 3. Distributions of $T_f(R)$ parameter estimates from a) Darwin 21 June 2011 to 22 July 2012, b) SGP 1 January 2015 to 2 May 2016, c) SGP 3 May 2016 to 5 June 2017. Outliers filtered using MAD ≥ 3 are marked in black.

Table 3. Best estimates of f and D together with their uncertainties for Doppler lidars at 5 ARM sites.

Location	Period	f	D	Available Profiles	Total estimates	Good estimates
Ascension	20160906–20170930	550±34 m	25.3±0.5 mm	18586	62	56
Darwin	20110621–20120722	590±62 m	24.0±0.7 mm	18988	3684	3528
Darwin	20120921–20140626	545±53 m	25.0±0.8 mm	30836	5046	4878
Graciosa	20150124–20161114	625±80 m	23.5±0.7 mm	31124	3737	3161
NSA	20140730–20171231	Infinity	11.8±1.5 mm	56832	1132	589
SGP	20150101–20160502	440±29 m	25.0±0.7 mm	22916	9198	8426
SGP	20160503–20170605	425±74 m	14.0±0.4 mm	14212	5814	5337

4 Results

4.1 Parameter estimation

We applied the $T_f(R)$ estimation method to Doppler lidars at 5 ARM atmospheric observatories. Figure 3a shows the distribution of f and D calculated for the Doppler lidar operating at Darwin in northern Australia between 21 June 2011 and 22 July 2012. This Doppler lidar is a Streamline and the distribution of f is positively skewed, as explained in section 3.2.2. The distribution displays a slightly wider peak than expected for a normal distribution.

Figure 3b shows the distribution of f and D for the Streamline Doppler lidar operating at SGP from 1 January 2015 to 2 May 2016. The distribution close to the peak is really tight, while the outliers have substantial spread. Many of the poor estimates responsible for the outlier spread occur during January and February in both years, while for the rest of the period the estimates are remarkably consistent. On 3 May 2016 the Doppler lidar at SGP was changed to a Streamline XR and Fig. 3c shows the distribution of f and D from 3 May 2016 to 5 June 2017. The change in instrument version, from Streamline to Streamline XR is clearly seen in the change in D, whereas the best estimate for f did not change. However, inspecting the data by eye would suggest a significantly shorter apparent focus, and the $T_f(R)$ calculated using the best estimates for f and D also exhibits a significantly shorter apparent focus. Consequently, the Streamline XR in SGP has been noted to suffer from poor SNR at the boundary layer top.

The bi-variate distributions of f and D show notable variations in how tight they are around the peak, and is likely a result of differences in data quality between the instruments. The best estimates of f and D and their uncertainties for all sites are presented in Table 3. The Doppler lidar measurements at Darwin were split into two periods, as there was a two month break in the measurements between these two periods. We performed the $T_f(R)$ parameter estimation separately for both periods. The best estimates from these periods differ from each other, which is expected as some adjustments were made to the instrument. The telescope focal length for this instrument is directly adjustable by any operator while the beam diameter is set by the manufacturer and is not modifiable by the operator. We note that the D estimates are the same for these two periods within the margin of error calculated.

For the sites and instruments selected here, only the Doppler lidar at NSA had f set to infinity. In fact, all Streamlines have D in the vicinity of 25 mm, whereas D for the Streamline XR versions is about half this. Nevertheless, the variation between instruments of the same version is not negligible and should be taken into account when calculating $T_f(R)$ and then attenuated backscatter.

The final step to obtain attenuated backscatter profiles is to apply a calibration constant, which can be achieved using the liquid cloud calibration method (Westbrook et al., 2010a; O'Connor et al., 2004).

The parameters f and D calculated for period 1 in Darwin have been used to derive $T_f(R)$ and the results applied in Fig. 4. This shows the utility of the method, able to provide reliable Doppler lidar attenuated backscatter profiles in Fig. 4b that show no over correction below 1 km and display similar in-cloud values to the ceilometer in Fig. 4c. It is expected that the aerosol attenuated backscatter coefficients will differ due to the different scattering properties of aerosol at the different wavelengths; the scattering properties of cloud droplets remain similar at the two wavelengths (O'Connor et al., 2004; Westbrook et al., 2010a).

4.2 Uncertainty

A computational method was used to calculate the uncertainty in the estimated $T_f(R)$ as it is a non-linear function of f and D. We used Monte Carlo simulation (MCS) (Morgan and Henrion, 1990) where a distribution of input values is fed into a model, here the effective receiver area equation (2), and the uncertainty is obtained from the distribution of the output. The input values can be created either from observed statistics, or by bootstrapping, i.e. re-sampling the data. We created three different sets of input values for our MCS:

1. Re-sampling the individual estimates of f and D provided directly by the $T_f(R)$ estimation method (i.e. those displayed in Fig. 3) after excluding outliers.

2. Generating the values from the statistics presented in Table 3, assuming that D and f^{-2} are normally distributed and independent, $N(f^{-2}, D)$.

3. Generating the values from statistics presented in Table 3, assuming D and f to be normally distributed and independent, $N(f, D)$.

For each set of input values, the relative uncertainty in $T_f(R)$ is calculated as

$$\sigma_{T_f}(R) = \frac{\sigma_{T_\phi}(R)}{T_f(R)}, \tag{9}$$

where $\sigma_{T_\phi}(R)$ is expressed in terms of the mean-squared deviation of the MCS-simulated telescope focus function, $T_\phi(R)$, from the best estimate of $T_f(R)$,

$$\sigma_{T_\phi}(R) = \sqrt{\frac{1}{N-1}\Sigma_{i=1}^{N}(T_{\phi_i}(R) - T_f(R))}, \tag{10}$$

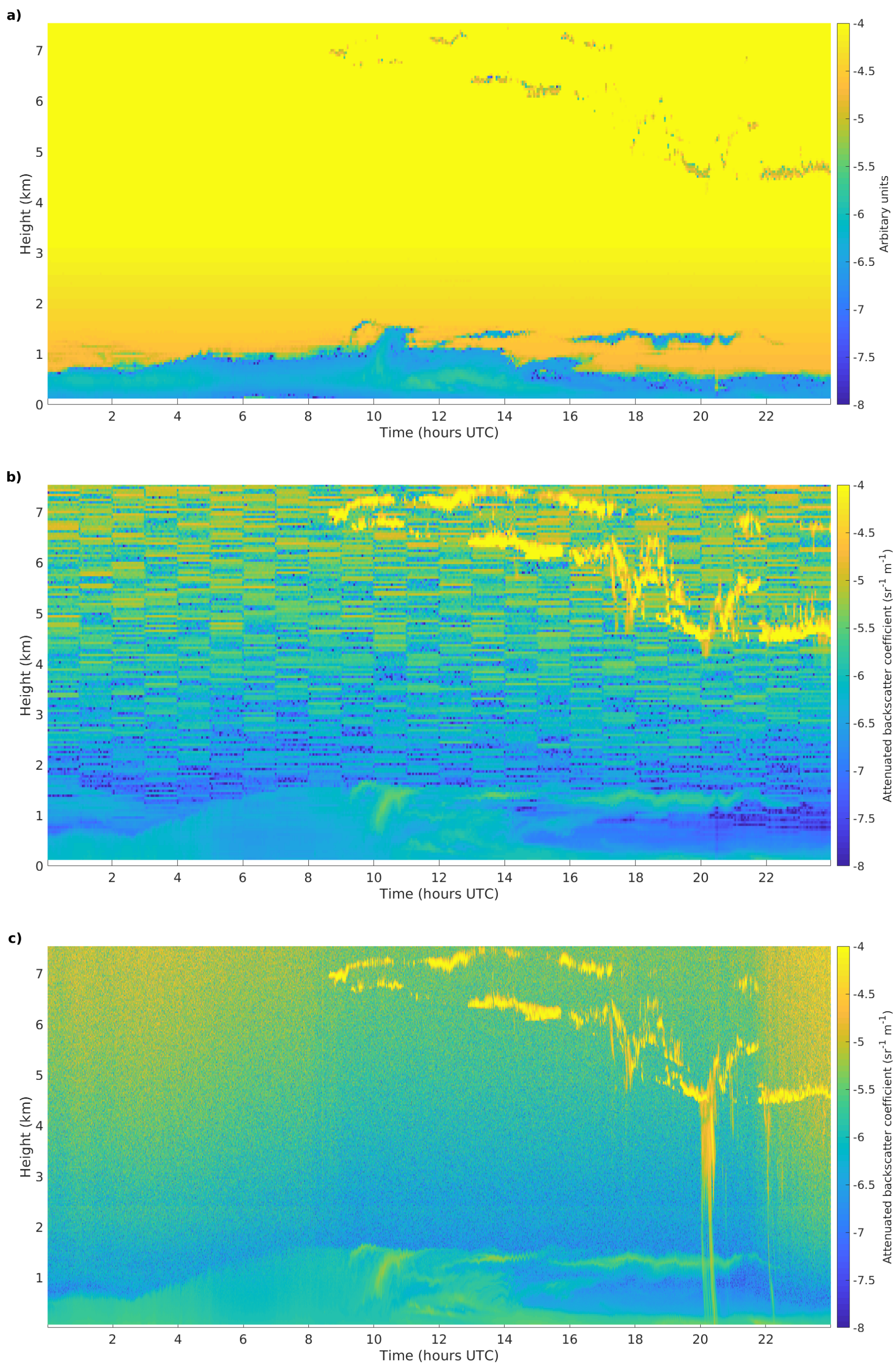

Figure 4. a) Doppler lidar attenuated backscatter coefficient assuming a generic $T_f(R)$, b) corrected Doppler lidar attenuated backscatter coefficient, c) ceilometer attenuated backscatter coefficient, from Darwin on 28 May 2012.

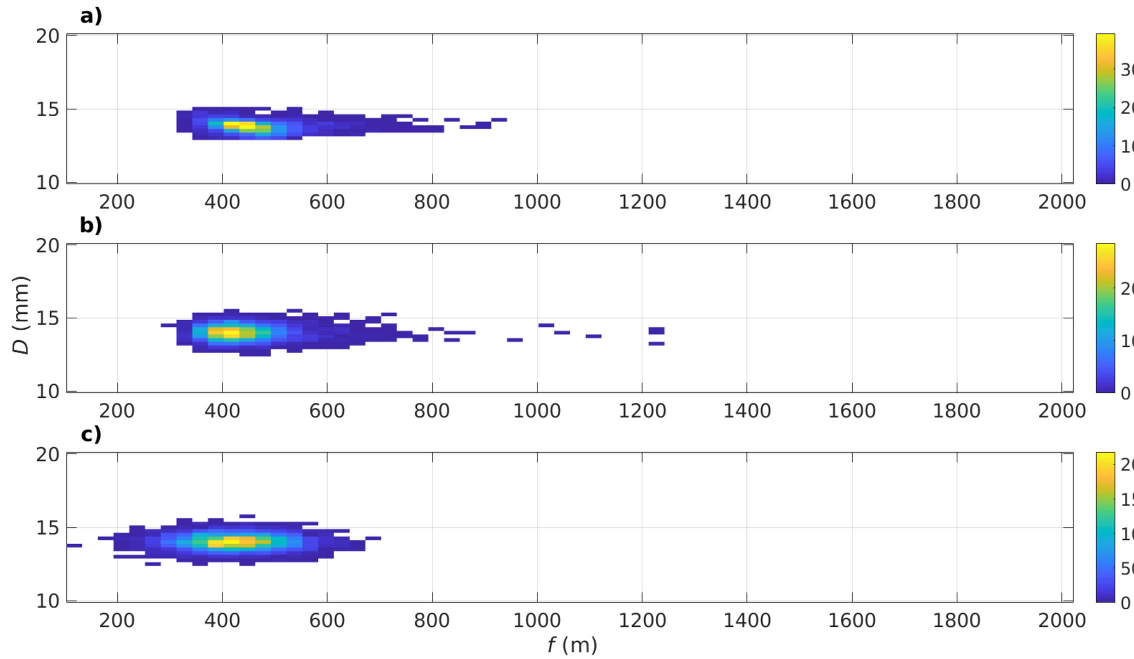

Figure 5. Distributions of the MCS input values used for calculating $\sigma_{T_f}(R)$. Values are obtained from a) re-sampling, b) assuming $N(f^{-2}, D)$, c) assuming $N(f, D)$. All distributions contain 5337 samples.

to avoid underestimating the uncertainty resulting from the asymmetry in $T_\phi(R)$. This also allows us to estimate the impact of refractive turbulence on the uncertainty estimate.

Examples of the three input parameter distributions are presented in figure 5. Re-sampling (Fig. 5a) is the most accurate method as it does not require assumptions about the parameter distributions and their independence. We recommend re-sampling as the primary method for uncertainty calculation. Using the $N(f^{-2}, D)$ distribution (Fig. 5b) produces a set of input values that appear to be a reasonable approximation, except that the distribution is not as tight around the peak. Using the $N(f, D)$ distribution (Fig. 5c) produces a set of input values that tend to over-emphasise shorter values of f, and under-emphasise higher values. We also note that the central bin of the re-sampled distribution contains 50% more samples than the central bin of the statistically-generated distributions do. We presume that this is a consequence of the variation in SNR not being necessarily normally distributed.

Figure 6a displays $\sigma_{T_f}(R)$ for Darwin showing the range-dependence of the uncertainty, with much larger uncertainties for ranges close to either side of the focus ($f = 590\ m$). The profile of uncertainties obtained with each set of MCS input values exhibit a similar shape, with $N(f^{-2}, D)$ being closer to re-sampling than $N(f, D)$ in the near field.

Figure 6b displays $\sigma_{T_f}(R)$ for the Doppler lidar at NSA which has f set to infinity, therefore $\sigma_{T_f}(R)$ is only dependent on the uncertainty in D. Note the reduced uncertainties around 200-400 m, which are expected when examining Fig. 1c.

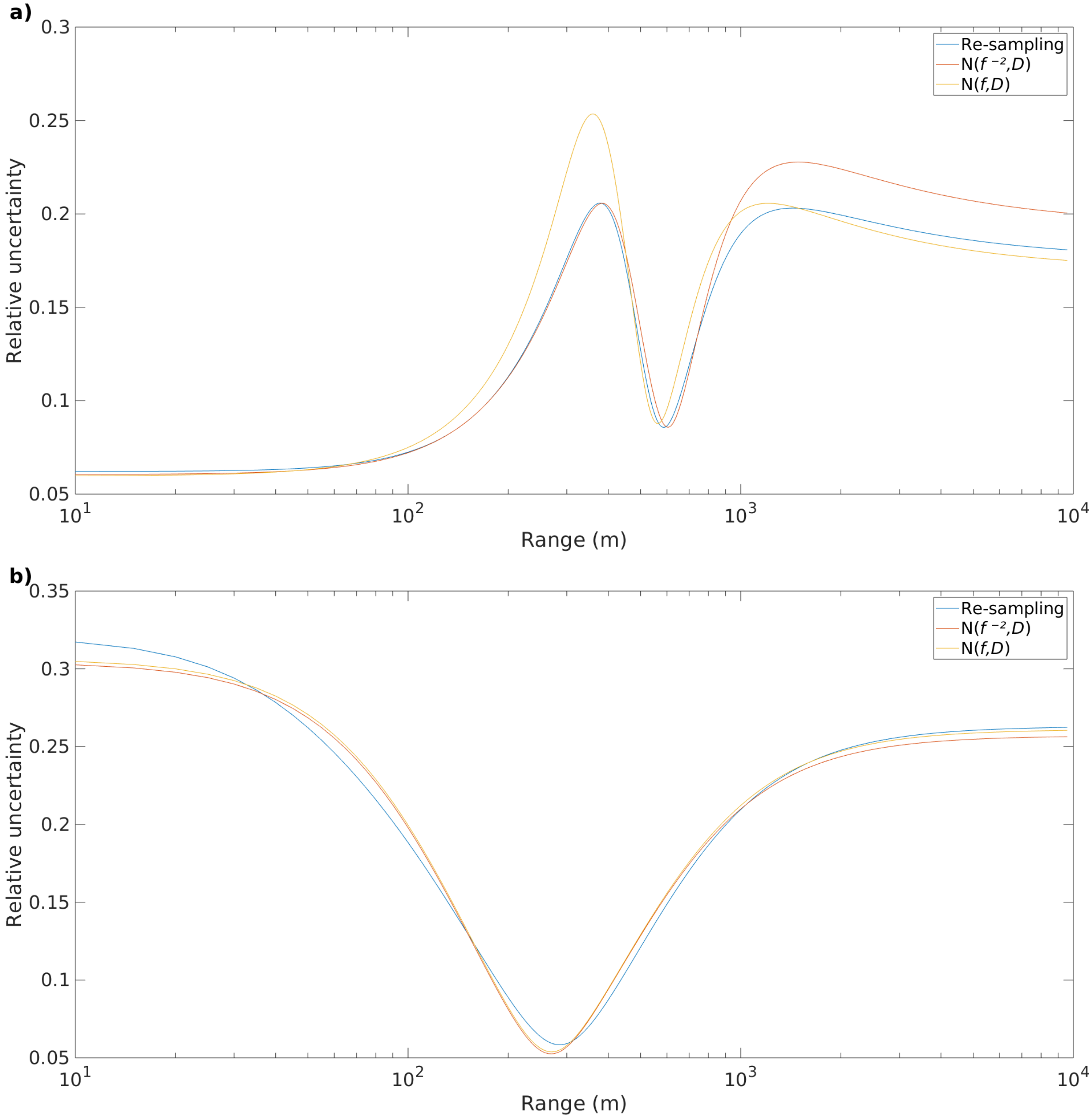

Figure 6. Relative telescope focus function uncertainties, $\sigma_{T_f}(R)$, generated using MCS with three different sets of input values for a) Darwin 21 June 2011 to 22 July 2012, and b) NSA 30 July 2014 to 31 December 2017

Table 4. $\sigma_{T_f}(R)$ uncertainty envelopes generated using MCS with three different sets of input values.

Location	Period	Re-sampling	$N(f^{-2},D)$	$N(f,D)$
Ascension	20160906–20170930	0.15	0.14	0.16
Darwin	20110621–20120722	0.21	0.23	0.25
Darwin	20120921–20140626	0.23	0.21	0.28
Graciosa	20150124–20161114	0.23	0.19	0.30
NSA	20140730–20171231	0.32	0.32	0.30
SGP	20150101–20160502	0.20	0.18	0.22
SGP	20160503–20170605	0.13	0.13	0.23

The largest value of $\sigma_{T_f}(R)$ provides the uncertainty envelope value for each site, which is presented in Table 4. Re-sampling provides values ranging from 0.12 for the updated instrument at SGP, to 0.32 at NSA. MCS values created using $N(f^{-2},D)$ provided similar values, whereas MCS using $N(f,D)$ often provided much larger uncertainties.

4.3 Impact of refractive turbulence

So far we have neglected the potential impact of turbulence on $T_f(R)$ arising from the refractive turbulent parameter, ρ_0, in (2). An expression for ρ_0 is given in Frehlich and Kavaya (1991),

$$\rho_0(R) = [Hk^2 \int_0^R {C_n}^2(z)(1-z/R)^{5/3}dz]^{-3/5}, \tag{11}$$

where $H = 2.914383$, $k = 2\pi/\lambda$, and ${C_n}^2(z)$ is the refractive turbulence at range z. We chose 3 profiles with constant ${C_n}^2(z)$, and a realistic vertical profile based on the most turbulent case presented by Roadcap and Tracy (2009). Figure 7 shows the impact that these different profiles have on $T_f(R)$, and the resulting re-sampling calculation of $\sigma_{T_f}(R)$ for two Doppler lidar instruments with different $T_f(R)$. Values of ${C_n}^2$ up to $10^{-14}m^{-2/3}$ have negligible impact on $T_f(R)$, and even the realistic profile only showed a slight increase in $\sigma_{T_f}(R)$ for the instrument with a focus set closer than infinity. This suggests that the impact of turbulence can be safely neglected for low values of ${C_n}^2$, and for most applications, can also be neglected when operating in the vertical. Hence, turbulence has no significant impact on the methodology described here for deriving the parameters f and D and their uncertainties from vertical profiles, but can be included for completeness.

However, it is clear that the turbulent impact should not be ignored when measuring at low elevation angles close to the horizon, where a profile similar to ${C_n}^2 = 10^{-13}m^{-2/3}$ may be possible. Fig. 7 shows that such a profile has a major impact on $T_f(R)$, especially in the far range. In these cases, the parameters f and D obtained from vertical measurements are still applicable, but $\rho_0(R)$ must also be calculated or estimated in order to derive the profile of attenuated backscatter, $\beta'(R)$.

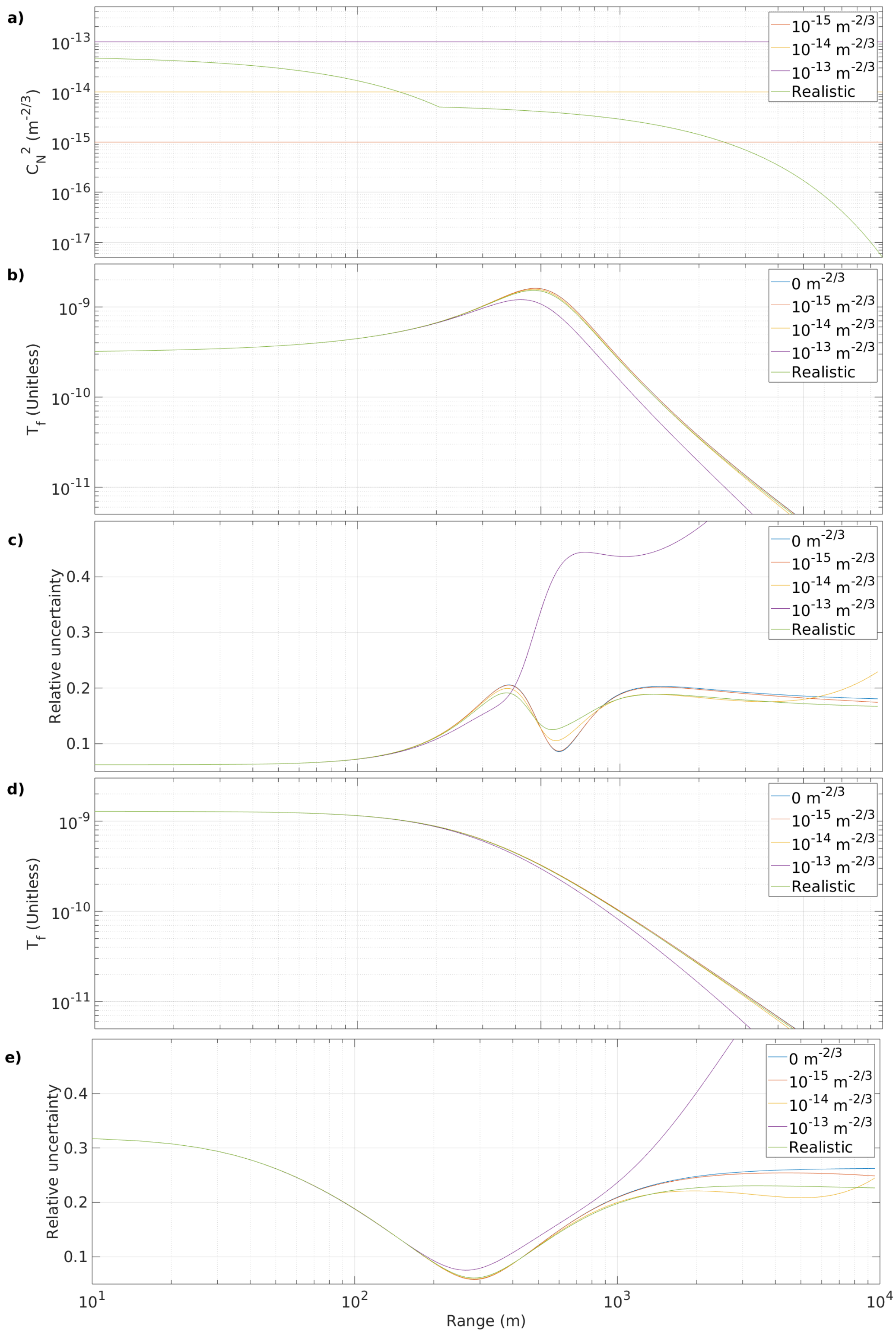

Figure 7. Impact of turbulent parameter, ρ_0, on telescope focus function, $T_f(R)$ and relative uncertainties, $\sigma_{T_f}(R)$, for different ${C_n}^2$ profiles. a) selected profiles of ${C_n}^2$ with range; b) $T_f(R)$ and c) $\sigma_{T_f}(R)$ for Darwin, 21 June 2011 to 22 July 2012; d) $T_f(R)$ and e) $\sigma_{T_f}(R)$ for NSA 30 July 2014 to 31 December 2017.

5 Validation

The liquid cloud calibration method (O'Connor et al., 2004; Westbrook et al., 2010a) is used to determine a calibration constant by integrating attenuated backscatter profiles containing fully attenuating liquid clouds, which have well-constrained apparent lidar ratio, ηS, where η is a multiple scattering factor and S is the lidar ratio. In the absence of multiple scattering, ηS can be assumed to be independent of the height of the cloud.

This calibration method can be used to evaluate the estimated $T_f(R)$ for Doppler lidar by checking whether the attenuated backscatter profiles obtained for the Doppler lidar after applying $T_f(R)$ indeed provide similar ηS values for liquid clouds at different heights.

Figure 8 shows examples of Doppler lidar attenuated backscatter profiles after calibration and the derived apparent lidar ratio at two sites, Darwin and NSA. These sites have different values of f, Darwin has $f = 590$ m and NSA has f set to infinity. For both cases, liquid clouds are present throughout the day with altitudes varying from 2 to 6 km. When fully attenuating liquid clouds are present, the apparent lidar ratio is close to the expected value of 20 sr, regardless of the height of the cloud, thus confirming that the method of estimating $T_f(R)$ is valid.

5.1 Limitations

Table 3 shows that the proportion of data that can be used for the $T_f(R)$ parameter estimation varies significantly from site to site. Over a third of the available profiles from SGP are used, whereas only 0.3% pass the filtering for Ascension. The lack of suitable profiles at Ascension is explained by the almost constant low cloud cover at this site, with very few profiles having a sufficient number of successive range gates.

Data quality is also a limiting factor so at sites with very low aerosol optical depth, AOD, such as NSA, the Doppler lidar SNR decreases so rapidly that again there are few profiles having a sufficient number of successive range gates. Low AOD also impacts the performance of the ceilometer, with 48% of the estimates at NSA discarded as outliers even after the initial filtering was performed. While the outlier removal can separate the good and the poor estimates, the largest uncertainty in D was at NSA. We attempted to perform the $T_f(R)$ parameter estimation on Doppler lidar from an ARM campaign in Cape Cod, but could not obtain reliable estimates due to the low SNR of the ceilometer data.

The $T_f(R)$ parameter estimation method is suitable only in situations where there is minimal difference in atmospheric extinction within the aerosol layer between the two instrument wavelengths of 910 nm and 1500 nm. Using AERONET AOD measurements collocated at the ARM atmospheric observatories, the median difference in AOD at 870 nm and 1640 nm varied from 0.016 and 0.027, which should correspond closely to what might be expected for the difference between ceilometer and Doppler lidar. Very occasional periods of notable AOD differences were observed at some sites, but including these profiles in timeseries extending beyond a year will have negligible impact on the $T_f(R)$ parameter best estimate. However, there were breaks in the AOD measurements, and some periods experiencing a significant differential extinction may have gone unnoticed. An additional filter using AERONET AOD measurements to remove profiles experiencing significant differential extinction could be included in Fig. 2 for those sites where this may be an issue.

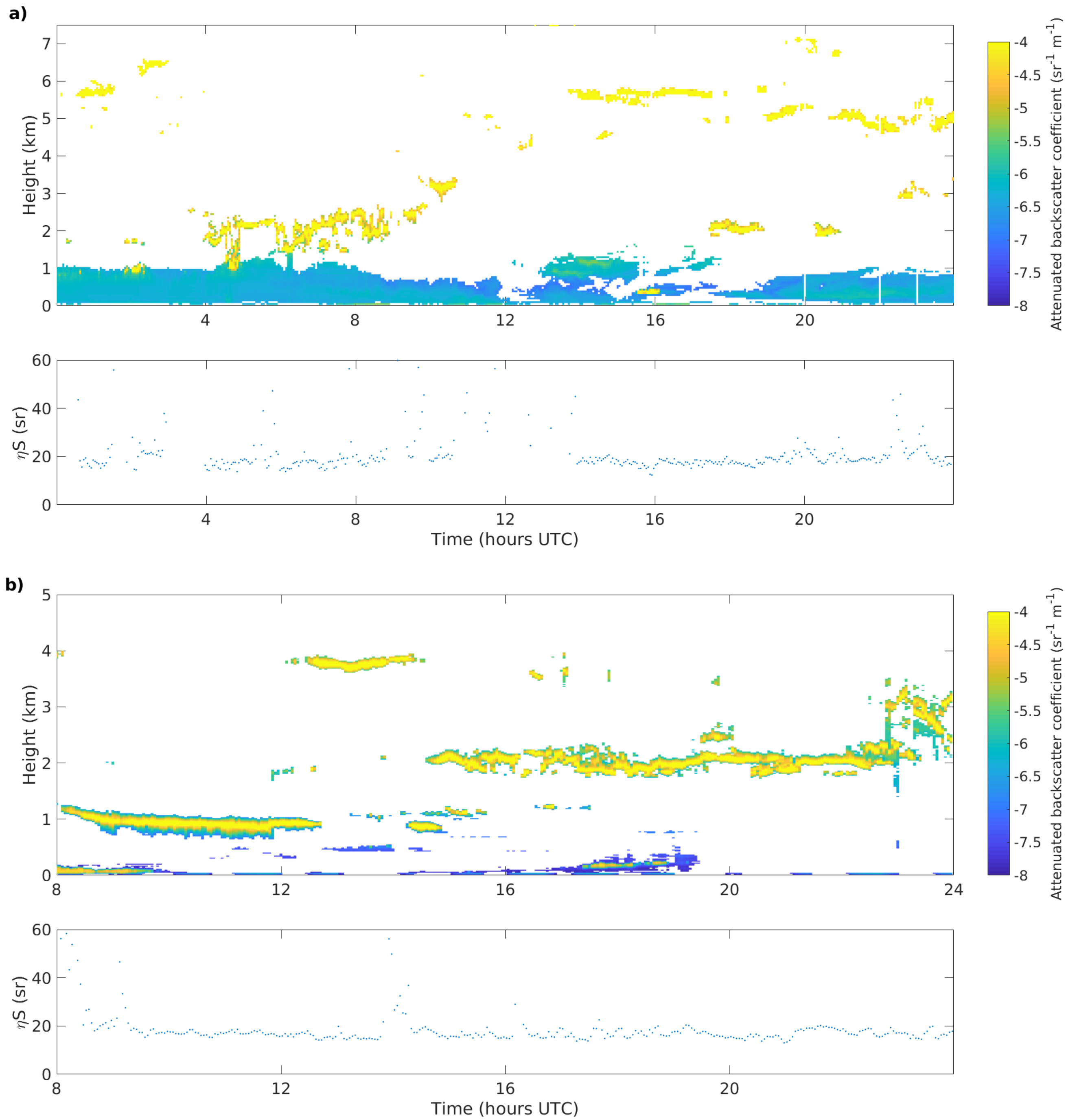

Figure 8. Doppler lidar attenuated backscatter coefficient and apparent lidar ratio, ηS, from a) Darwin on 8 May 2012, b) NSA on 20 August 2014.

6 Conclusions

We have developed a method for deriving the telescope focus function and its uncertainty for pulsed heterodyne Doppler lidars, and applied the method to Halo Photonics Streamline and XR Doppler lidars. The method compares profiles of the Doppler lidar SNR to profiles of attenuated backscatter coefficient from a collocated ceilometer, producing estimates for two parameters of the $T_f(R)$; the effective focal length for the telescope, f, and the $1/e^2$ effective diameter of a Gaussian beam, D. This method was developed because it also provides uncertainties in f, D and $T_f(R)$, necessary for quantitative use of the subsequently derived attenuated backscatter profiles. The method can be used to check the manufacturer specifications for these parameters, calculate them if not known, and also check their stability over time.

The method was applied to data from Doppler lidars with different configurations deployed at 5 ARM sites. Relative uncertainties in f for these instruments ranged from 6% to 17% with the median uncertainty being 10%; the relative uncertainty in D ranged from 2% to 12% with median of 3%. The uncertainty in $T_f(R)$ was calculated using Monte Carlo simulation, using 3 methods to prepare the input values. We recommend the direct re-sampling method, but reasonable results were obtained used statistically-derived input values assuming a normal distribution. The envelope of relative uncertainties in $T_f(R)$ ranged from 13% to 32%, and depend on both the instrument configuration and the instrument location. We also show that, even for a Doppler lidar with the focus set at infinity, uncertainty remains in estimating $T_f(R)$ arising from the uncertainty in D. The method was validated by calculating the apparent lidar ratio of fully attenuating liquid clouds from $T_f(R)$ corrected profiles of Doppler lidar attenuated backscatter.

The impact of turbulence on $T_f(R)$ was also investigated and was found to have no significant impact on the methodology described here for deriving the parameters f and D and their uncertainties from vertical profiles. However, the turbulent impact should not be ignored when measuring at low elevation angles close to the horizon, as it can modify $T_f(R)$ considerably, especially in the far range. In these cases, the parameters f and D obtained from vertical measurements are still applicable, but the turbulent contribution to $T_f(R)$ should included when deriving the attenuated backscatter coefficient.

The $T_f(R)$ estimation method is suitable only for conditions where the differential extinction at the two wavelengths of the Doppler lidar and the ceilometer is small, which can be identified, for example, using AOD from co-located AERONET observations.

Competing interests. The authors declare that they have no conflict of interest.

Acknowledgements. This study was supported by the U.S. Department of Energy's Atmospheric System Research (ASR), an Office of Science, Office of Biological and Environmental Research (BER) program, under Contract DE-SC0017338. The Doppler lidar and ceilometer data used in this study were obtained from the Atmospheric Radiation Measurement (ARM) user facility, managed by the Office of Biological and Environmental Research for the U.S. Department of Energy Office of Science.

References

Chouza, F., Reitebuch, O., Groß, S., Rahm, S., Freudenthaler, V., Toledano, C., and Weinzierl, B.: Retrieval of aerosol backscatter and extinction from airborne coherent Doppler wind lidar measurements, Atmos. Meas. Tech., 8, 2909–2926, https://doi.org/10.5194/amt-8-2909-2015, https://www.atmos-meas-tech.net/8/2909/2015/, 2015.

Engelmann, R., Wandinger, U., Ansmann, A., Müller, D., Žeromskis, E., Althausen, D., and Wehner, B.: Lidar observations of the vertical aerosol flux in the planetary boundary layer, Journal of Atmospheric and Oceanic Technology, 25, 1296–1306, https://doi.org/10.1175/2007JTECHA967.1, 2008.

Flentje, H., Heese, B., Reichardt, J., and Thomas, W.: Aerosol profiling using the ceilometer network of the German Meteorological Service, Atmospheric Measurement Techniques Discussions, 3, 3643–3673, https://doi.org/10.5194/amtd-3-3643-2010, https://www.atmos-meas-tech-discuss.net/3/3643/2010/, 2010.

Frehlich, R. G. and Kavaya, M. J.: Coherent laser radar performance for general atmospheric refractive turbulence, Appl. Opt., 30, 5325–5352, https://doi.org/10.1364/AO.30.005325, http://ao.osa.org/abstract.cfm?URI=ao-30-36-5325, 1991.

Hannon, S. M., Thomson, J. A. L., and Smith, D. D.: Plume detection and tracking using Doppler lidar aerosol and wind data, in: Application of Lidar to Current Atmospheric Topics III, edited by Sedlacek III, A. J. and Fischer, K. W., vol. 3757, pp. 28 – 39, International Society for Optics and Photonics, SPIE, https://doi.org/10.1117/12.366435, https://doi.org/10.1117/12.366435, 1999.

Harvey, N. J., Hogan, R. J., and Dacre, H. F.: A method to diagnose boundary-layer type using Doppler lidar, Quarterly Journal of the Royal Meteorological Society, 139, 1681–1693, https://doi.org/10.1002/qj.2068, 2013.

Henderson, S. W., Gatt, P., Rees, D., and Huffaker, R. M.: Wind Lidar, in: Laser Remote Sensing, edited by Fujii, T. and Fukuchi, T., pp. 469–722, CRC Taylor and Francis, 2005.

Hill, C.: Coherent focused lidars for Doppler sensing of aerosols and wind, Remote Sensing, 10, 466, https://doi.org/10.3390/rs10030466, http://dx.doi.org/10.3390/rs10030466, 2018.

Hirsikko, A., O'Connor, E. J., Komppula, M., Korhonen, K., Pfüller, A., Giannakaki, E., Wood, C. R., Bauer-Pfundstein, M., Poikonen, A., Karppinen, T., Lonka, H., Kurri, M., Heinonen, J., Moisseev, D., Asmi, E., Aaltonen, V., Nordbo, A., Rodriguez, E., Lihavainen, H., Laaksonen, A., Lehtinen, K. E. J., Laurila, T., Petäjä, T., Kulmala, M., and Viisanen, Y.: Observing wind, aerosol particles, cloud and precipitation: Finland's new ground-based remote-sensing network, Atmos. Meas. Tech., 7, 1351–1375, https://doi.org/10.5194/amt-7-1351-2014, 2014.

Hogan, R. J., Illingworth, A. J., O'connor, E. J., and Baptista, J. P. V. P.: Characteristics of mixed-phase clouds. II: A climatology from ground-based lidar, Quarterly Journal of the Royal Meteorological Society, 129, 2117–2134, https://doi.org/10.1256/qj.01.209, https://rmets.onlinelibrary.wiley.com/doi/abs/10.1256/qj.01.209, 2003.

Hu, Q., Rodrigo, P. J., Iversen, T. F. Q., and Pedersen, C.: Investigation of spherical aberration effects on coherent lidar performance, Opt. Express, 21, 25 670–25 676, https://doi.org/10.1364/OE.21.025670, http://www.opticsexpress.org/abstract.cfm?URI=oe-21-22-25670, 2013.

Huber, P. J. and Ronchetti, E.: Robust Statistics, chap. 5, pp. 105–123, John Wiley & Sons, Ltd, https://doi.org/10.1002/9780470434697.ch5, https://onlinelibrary.wiley.com/doi/abs/10.1002/9780470434697.ch5, 2009.

Illingworth, A. J., Cimini, D., Haefele, A., Haeffelin, M., Hervo, M., Kotthaus, S., Löhnert, U., Martinet, P., Mattis, I., O'Connor, E. J., and Potthast, R.: How can existing ground-based profiling instruments improve European weather forecasts?, Bull. Amer. Meteorol. Soc., 100, 605–619, https://doi.org/10.1175/BAMS-D-17-0231.1, https://doi.org/10.1175/BAMS-D-17-0231.1, 2019.

Kotthaus, S. and Grimmond, C. S. B.: Atmospheric boundary-layer characteristics from ceilometer measurements. Part 1: A new method to track mixed layer height and classify clouds, Quarterly Journal of the Royal Meteorological Society, 144, 1525–1538, https://doi.org/10.1002/qj.3299, https://rmets.onlinelibrary.wiley.com/doi/abs/10.1002/qj.3299, 2018.

Leys, C., Ley, C., Klein, O., Bernard, P., and Licata, L.: Detecting outliers: Do not use standard deviation around the mean, use absolute deviation around the median, Journal of Experimental Social Psychology, 49, 764 – 766, https://doi.org/https://doi.org/10.1016/j.jesp.2013.03.013, http://www.sciencedirect.com/science/article/pii/S0022103113000668, 2013.

Lolli, S., D'Adderio, L. P., Campbell, J. R., Sicard, M., Welton, E. J., Binci, A., Rea, A., Tokay, A., Comerón, A., Barragan, R., Baldasano, J. M., Gonzalez, S., Bech, J., Afflitto, N., Lewis, J., and Madonna, F.: Vertically resolved precipitation intensity retrieved through a synergy between the ground-Based NASA MPLNET lidar network measurements, surface disdrometer datasets and an analytical model solution, Remote Sensing, 10, 1102, https://doi.org/10.3390/rs10071102, http://dx.doi.org/10.3390/rs10071102, 2018.

Manninen, A. J., O'Connor, E. J., Vakkari, V., and Petäjä, T.: A generalised background correction algorithm for a Halo Doppler lidar and its application to data from Finland, Atmos. Meas. Tech., 9, 817–827, https://doi.org/10.5194/amt-9-817-2016, 2016.

Manninen, A. J., Marke, T., Tuononen, M., and O'Connor, E. J.: Atmospheric boundary layer classification with Doppler lidar, Journal of Geophysical Research: Atmospheres, 123, 8172–8189, https://doi.org/10.1029/2017JD028169, https://doi.org/10.1029/2017JD028169, 2018.

Mather, J. H., Turner, D. D., and Ackerman, T. P.: Scientific maturation of the ARM Program, Meteorological Monographs, 57, 4.1–4.19, https://doi.org/10.1175/AMSMONOGRAPHS-D-15-0053.1, 2016.

Morgan, M. G. and Henrion, M.: Uncertainty: A guide to dealing with uncertainty in quantitative risk and policy analysis, p. 172–219, Cambridge University Press, https://doi.org/10.1017/CBO9780511840609.009, 1990.

O'Connor, E. J., Illingworth, A. J., and Hogan, R. J.: A technique for autocalibration of cloud lidar, Journal of Atmospheric and Oceanic Technology, 21, 777–786, https://doi.org/10.1175/1520-0426(2004)021<0777:ATFAOC>2.0.CO;2, https://doi.org/10.1175/1520-0426(2004)021<0777:ATFAOC>2.0.CO;2, 2004.

Pearson, G., Davies, F., and Collier, C.: An analysis of the performance of the UFAM pulsed Doppler lidar for observing the boundary layer, Journal of Atmospheric and Oceanic Technology, 26, 2009.

Pearson, G. N., Roberts, P. J., Eacock, J. R., and Harris, M.: Analysis of the performance of a coherent pulsed fiber lidar for aerosol backscatter applications, Appl. Opt., 41, 6442–6450, https://doi.org/10.1364/AO.41.006442, http://ao.osa.org/abstract.cfm?URI=ao-41-30-6442, 2002.

Roadcap, J. R. and Tracy, P.: A preliminary comparison of daylit and night $\mathrm{C_n}^2$ profiles measured by thermosonde, Radio Science, 44, https://doi.org/10.1029/2008RS003921, https://agupubs.onlinelibrary.wiley.com/doi/abs/10.1029/2008RS003921, 2009.

Rye, B. J. and Hardesty, R. M.: Discrete spectral peak estimation in incoherent backscatter heterodyne lidar. I. Spectral accumulation and the Cramer-Rao lower bound, IEEE Transactions on Geoscience and Remote Sensing, 31, 16–27, https://doi.org/10.1109/36.210440, 1993.

Tonttila, J., O'Connor, E. J., Hellsten, A., Hirsikko, A., O'Dowd, C., Järvinen, H., and Räisänen, P.: Turbulent structure and scaling of the inertial subrange in a stratocumulus-topped boundary layer observed by a Doppler lidar, Atmos. Chem. Phys, 15, 5873–5885, https://doi.org/10.5194/acp-15-5873-2015, https://www.atmos-chem-phys.net/15/5873/2015/, 2015.

Träumner, K., Handwerker, J., Wieser, A., and Grenzhäuser, J.: A Synergy Approach to Estimate Properties of Raindrop Size Distributions Using a Doppler Lidar and Cloud Radar, Journal of Atmospheric and Oceanic Technology, 27, 1095–1100, https://doi.org/10.1175/2010JTECHA1377.1, 2010.

Tucker, S. C., Senff, C. J., Weickmann, A. M., Brewer, W. A., Banta, R. M., Sandberg, S. P., Law, D. C., and Hardesty, R. M.: Doppler lidar estimation of mixing height using turbulence, shear, and aerosol Profiles, Journal of Atmospheric and Oceanic Technology, 26, 673–688, https://doi.org/10.1175/2008JTECHA1157.1, 2009.

Van Tricht, K., Gorodetskaya, I. V., Lhermitte, S., Turner, D. D., Schween, J. H., and Van Lipzig, N. P. M.: An improved algorithm for polar cloud-base detection by ceilometer over the ice sheets, Atmos. Meas. Tech., 7, 1153–1167, https://doi.org/10.5194/amt-7-1153-2014, https://www.atmos-meas-tech.net/7/1153/2014/, 2014.

Westbrook, C., Illingworth, A., O'Connor, E., and Hogan, R.: Doppler lidar measurements of oriented planar ice crystals falling from supercooled and glaciated layer clouds, Quarterly Journal of the Royal Meteorological Society, 136, https://doi.org/10.1002/qj.528, 2010a.

Westbrook, C. D., Hogan, R. J., O'Connor, E. J., and Illingworth, A. J.: Estimating drizzle drop size and precipitation rate using two-colour lidar measurements, Atmos. Meas. Tech., 3, 671–681, https://doi.org/10.5194/amt-3-671-2010, https://www.atmos-meas-tech.net/3/671/2010/, 2010b.

Zhao, Y., Post, M. J., and Hardesty, R. M.: Receiving efficiency of monostatic pulsed coherent lidars. 1: Theory, Appl. Opt., 29, 4111–4119, https://doi.org/10.1364/AO.29.004111, http://ao.osa.org/abstract.cfm?URI=ao-29-28-4111, 1990.